4-2-2022

# Atmospheric Plasma Spraying to Fabricate Metal-Supported Solid Oxide Fuel Cells With Open-Channel Porous Metal Support

Jie Lin

Haixia Li

Wanhua Wang

Peng Qiu

Greg Tao

*See next page for additional authors*



## Publication Info

Published in *Journal of the American Ceramic Society*, Volume 106, Issue 1, 2022, pages 68-78.

Received: 1 December 2021 | Revised: 28 February 2022 | Accepted: 7 March 2022

DOI: 10.1111/jace.18450

Journal of the American Ceramic Society

SPECIAL ISSUE ARTICLE

# Atmospheric plasma spraying to fabricate metal-supported solid oxide fuel cells with open-channel porous metal support

**Jie Lin**[1] | **Haixia Li**[1] | **Wanhua Wang**[1] | **Peng Qiu**[2] | **Greg Tao**[3] | **Kevin Huang**[1] | **Fanglin Chen**[1]

[1]Department of Mechanical Engineering, University of South Carolina, Columbia, South Carolina, USA

[2]School of Materials Science and Engineering, Shandong University of Science and Technology, Qingdao, People's Republic of China

[3]Chemtronergy, LLC, Salt Lake City, Utah, USA

**Correspondence**
Fanglin Chen, Department of Mechanical Engineering, University of South Carolina, Columbia, SC 29208, United States.
Email: chenfa@cec.sc.edu

**Funding information**
US Department of Energy, Grant/Award Numbers: DE-EE0009427, DE-FE0031670

## Abstract

Metal-supported solid oxide fuel cells (MS-SOFCs) have been fabricated by applying phase-inversion tape-casting and atmospheric plasma spraying (APS). The effect of the binder amount of the phase-inversion slurries on the microstructure development of the 430L stainless steel metal support was investigated. The pore structures, the viscosity of the slurry, porosity and permeability of the as-prepared metal supports are significantly influenced by the amount of the binder. NiO–scandia-stabilized zirconia (ScSZ) anode, ScSZ electrolyte and $La_{0.6}Sr_{0.4}Co_{0.2}Fe_{0.8}O_{3-\delta}$ (LSCF) cathode layers were consecutively deposited on the metal support with an ideal microstructure by APS process. The effect of plasma power of the APS on the microstructure of the electrolyte and cathode was investigated. A dense electrolyte layer and a porous cathode layer were successfully obtained at 40 and 6 kW of the APS plasma power, respectively. MS-SOFCs, with a cell configuration of 430L/Ni-ScSZ/ScSZ/LSCF, achieved a maximum cell power density of 1079 mW $cm^{-2}$ at 700°C using humidified $H_2$ as fuel and ambient air as oxidant. The corresponding ohmic resistance and total resistance of MS-SOFCs was 0.14 and 0.32 Ω $cm^2$, respectively. This work demonstrates the feasibility of fabricating high-performance MS-SOFCs with economical and scalable techniques.

**KEYWORDS**
atmospheric plasma spraying, metal-supported solid oxide fuel cells, phase-inversion tape casting, plasma power

## 1 | INTRODUCTION

Metal-supported solid oxide fuel cells (MS-SOFCs) have been recognized as a versatile energy conversion device for a number of advantages over the state-of-the-art cermet anode–supported SOFCs, including low-cost structural materials, high mechanical strength, excellent sealing efficiency, improved thermal shock resistance and extremely

fast start-up capability.[1–3] Anode-supported planar SOFCs are typically fabricated using tape casting and screen printing where co-sintering of the anode/electrolyte bilayers is first performed, followed by a separate thermal fabrication of the cathode.[4,5] However, it is very difficult to manufacture MS-SOFCs using the anode-supported SOFC-manufacturing processes without oxidizing the metal substrate or significantly changing cell component materials properties. For example, sintering the cathode material under in air would invoke severe oxidation of metal substrates such as stainless steel.[6] Meanwhile, the use of high-temperature sintering to densify the electrolyte typically leads to significant interdiffusion between Fe and Cr from the stainless steel and Ni from the anode, which, in turn, results in high cell resistance, low cell power density and a rapid performance degradation of MS-SOFCs.[7,8]

One major focus of current SOFC development is to lower the cell operating temperatures in order to reduce the cost and improve the durability of the SOFC systems. A mixed ionic–electronic conductor such as $La_{0.6}Sr_{0.4}Co_{0.2}Fe_{0.8}O_{3-\delta}$ (LSCF) is widely used as an SOFC cathode material, which exhibits excellent performances at intermediate temperatures due to its high-catalytic activity for oxygen reduction and oxygen ion mobility.[9–11] However, LSCF usually reacts with Zr-based electrolytes to form insulating $La_2ZrO_7$ or $SrZrO_3$ phases at the electrolyte/cathode interface during the preparation or operation of SOFCs at elevated temperatures.[12] Therefore, a diffusion barrier layer, such as doped ceria, is usually added between the electrolyte and the cathode to prevent insulating phase formation during high-temperature process.[13–15] However, the introduction of a diffusion barrier layer has added complexity to the cell fabrication process and incurred additional ohmic loss in the cell.

To overcome the aforementioned challenges, the atmospheric plasma spraying (APS) technique has been explored for manufacturing SOFCs.[16–19] The APS process utilizes high-temperature plasma flame created by a plasma torch to fully or partially melt particles that are subsequently deposited on a substrate.[20,21] Compared with other deposition methods such as chemical vapor deposition,[22] pulsed laser deposition,[23] vacuum plasma spraying[24,25] and suspension plasma spray,[26] APS offers an ideal cost-effective solution for iterative processes at high volume productions and fast production rates, thus minimizing the potential reactions/interdiffusions among different SOFC layers at lower temperatures without additional heat treatment. Furthermore, the APS process can easily control the composition and microstructure of sprayed layers by adjusting the spraying parameters.

MS-SOFCs fabricated using APS have been reported, mainly on ceramic powders deposited on a porous metal substrate, which was fabricated by dry pressing or tape casting. Pore formers (graphite, starch or polystyrene) were typically used to control the metallic support microstructure, forming a sponge-like microstructure with random and irregular pores.[6] However, subsequent heat treatment in reducing conditions to remove pore formers may result in carbon residues on the metallic support, due to the pyrolysis of the pore formers. In addition, sponge-like morphology is also not beneficial to gas diffusion because of high tortuosity factor, consequently limiting the cell electrochemical performance.[27,28] Recently, the phase-inversion tape-casting method that combines tape casting and phase inversion has been utilized to optimize the cermet anode microstructure in planar anode-supported SOFCs, exhibiting high performance and low concentration polarization resistance.[29–32] The cermet anode support fabricated by phase-inversion tape-casting method has a unique three-layer microstructure, including a skin, a finger-like and a sponge-like layer. The large straight pores perpendicular to the ceramic anode support thickness direction in the finger-like layer are expected to facilitate gas transport. Consequently, metal support with such a unique microstructure, resulting from the phase-inversion tape-casting method, may reduce the concentration polarization and enhance the cell performance of MS-SOFCs.

In this work, the phase-inversion tape-casting method has been used to produce planar metal support. Stainless steel 430L powders are used to prepare the slurries. The pore formation mechanism has been evaluated using the viscous fingering mechanism, and the effects of binder amount on the microstructure are systematically investigated. The APS process was used to fabricate porous anode, dense electrolyte and porous cathode on top of the porous metal substrate. The cell microstructure and electrochemical performances were evaluated as a function of plasma power of the APS.

## 2 | EXPERIMENTAL SECTION

### 2.1 | Materials

Stainless steel 430L powders (US Research Nanomaterials Inc., USA) were used as the metal support materials. These powders have a d50 particle size of about 10 $\mu$m and spherical granule morphology, as revealed in Figure 1A. Polyethersulfone (PESf, Veradel 3000P, Solvay Specialty Polymers, USA), *N*-methyl-2-pyrrolidone (NMP, HPLC grade, Sigma-Aldrich, USA) and polyvinylpyrrolidone (PVP, VWR Chemicals, USA) were used as the polymer binder, solvent and dispersant, respectively. Agglomerated NiO–scandia-stabilized zirconia (ScSZ) powders (10 mol% $Sc_2O_3$–90 mol% $ZrO_2$) (Qingdao Tianyao Materials Co., Ltd., China) with an NiO:ScSZ weight ratio of 60:40 was

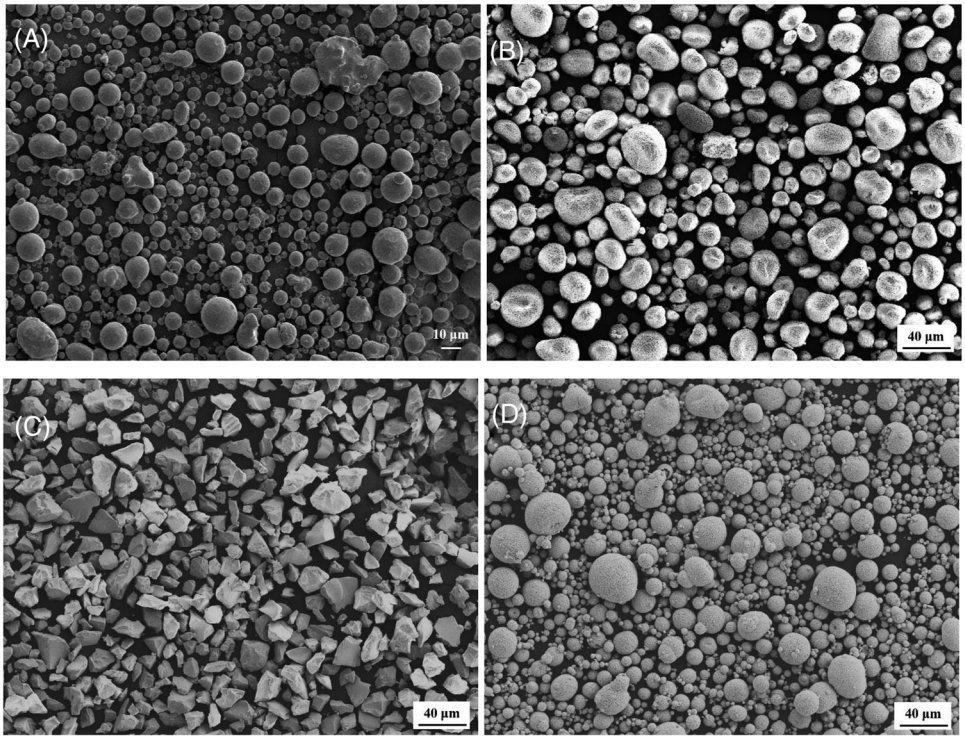


**FIGURE 1** SEM images of the starting materials: (A) 430L powders (B) NiO–ScSZ, (C) ScSZ and (D) LSCF. LSCF, $La_{0.6}Sr_{0.4}Co_{0.2}Fe_{0.8}O_{3-\delta}$; ScSZ, scandia-stabilized zirconia; SEM, scanning electron microscopy

employed as the anode materials. Figure 1B shows the morphology of NiO–ScSZ powder with particles around 10–40 $\mu$m in diameters and good flowability. Fused and crushed ScSZ powders (Daiichi Kigenso Kagaku Kogyo Co., Ltd., Japan) were used as the electrolyte feedstock material that has a particle size in the range of 10–30 $\mu$m and displays an irregular shape (Figure 1C). In addition, agglomerated LSCF (HC Starck, Germany) spherical powers with a particle size of 10–50 $\mu$m were used as the cathode material (Figure 1D). To avoid clogging, all powders were dried prior to the spraying.

**TABLE 1** Composition of the casting slurry for preparation of the metal support

| Compositions (wt.%) | | | | | |
|---|---|---|---|---|---|
| NMP | PESf | PVP | Solid loading | NMP:PESf:PVP | Sample ID |
| 24.83 | 4.14 | 1.03 | 70 | 6:1:0.25 | M1 |
| 24 | 4.8 | 1.2 | 70 | 5:1:0.25 | M2 |
| 23.48 | 5.22 | 1.30 | 70 | 4.5:1:0.25 | M3 |
| 22.86 | 5.71 | 1.43 | 70 | 4:1:0.25 | M4 |
| 21.18 | 7.06 | 1.76 | 70 | 3:1:0.25 | M5 |

Abbreviation: NMP, *N*-methyl-2-pyrrolidone; PESf, polyethersulfone; PVP, polyvinylpyrrolidone.

## 2.2 | Fabrication of metal support

430L stainless steel metal support was prepared using the phase-inversion tape-casting process.[32] PESf and PVP were first dissolved in an NMP solvent to form a homogeneous solution, and 430L stainless steel powders were subsequently added. The composition of the slurries is summarized in Table 1. The slurries were ball-milled for 24 h. Prior to tape casting, the slurries were de-aired using a vacuum pump until no bubbles were observed. The slurries were then casted onto a Mylar carrier film via a doctor blade with a 0.9 mm gap, and the casted metal support was immediately transferred into a water bath for 12 h, where the organic solvent exchanged with water to complete the solidification process. The resultant green metal support tapes were punched into metal pellets with a diameter of about 15 mm and dried at room temperature. The metal pellets were then heat-treated in a box muffle furnace in air at 500 °C for 1 h with a 1 °C $min^{-1}$ heating rate to remove the organic binders, and subsequently heat-treated at 1250 °C for 3.5 h in a tubular furnace under the atmosphere of 5% hydrogen/nitrogen.

## 2.3 | Cell fabrication

The optimized metal disk with a thickness of 0.75 mm and a diameter of 13 mm was used as metal support to

**TABLE 2** Plasma-spraying parameters for the electrolyte and cathode

| Parameters | ScSZ | LSCF |
|---|---|---|
| Plasma power (kW) | 32, 36, 40 | 6, 9, 12 |
| Primary gas (Ar) (L $min^{-1}$) | 60 | 60 |
| Secondary gas (He) (L $min^{-1}$) | 6 | 6 |
| Powder feed rate (g $min^{-1}$) | 5 | 5 |
| Spray distance (mm) | 70 | 150 |

Abbreviation: LSCF, $La_{0.6}Sr_{0.4}Co_{0.2}Fe_{0.8}O_{3-\delta}$; ScSZ, scandia-stabilized zirconia.

fabricate SOFCs using APS. The anode functional layer was deposited on the metal support using an SG-100 spray gun (Praxair Surface Technologies, USA) at a plasma arc power of 24 kW and a feed rate of 3 g $min^{-1}$. Argon (Ar) was used as a primary gas, and helium (He) was used as a secondary and carrier gas. The pressures of primary and secondary gas were fixed at 1.0 and 0.8 MPa, respectively. The flow rates of Ar and He were set at 60 and 6 L $min^{-1}$, respectively. The spray distance was 150 mm. To investigate the effect of plasma arc power on the microstructure and the property of the electrolyte and cathode, different plasma powers were applied to fabricate the electrolyte and the cathode coatings. The detailed plasma spray parameters for the electrolyte and the cathode fabrication are listed in Table 2.

## 2.4 | Characterization of metal substrate with metal-supported solid oxide fuel cells

Rheological properties of the slurries were determined using an AR Rheometer (Model AR2000 ex, TA Instrument Co., USA) at 25 °C. After the slurries were presheared for 30 s, the measurements were performed by stepping up to high shearing rates. The porosity of as-prepared metal supports was measured by the Archimedes method in water. The gas permeability was tested using a homemade equipment. Nitrogen was fed into the cylinder at various pressures, and the amount of permeated $N_2$ was measured with a flowmeter. Microstructure characterization is performed using scanning electron microscopy (SEM, Zeiss Ultra Plus FESEM). To investigate the performance of the electrolyte, half-cells with Pt as the air electrode were sealed to an alumina tube with conductive adhesive (DAD-87, Shanghai Research Institute of Synthetic Resins, China). High-temperature ceramic adhesives (552–1105, Aremco, USA) were then applied outside the attached cells to avoid gas leaking. Silver paste (Sino-platinum Metals Co., Ltd., China) was used as the current collector on both anodes and air electrodes with Ag wire as the lead wire. Humidified (3 vol% $H_2O$) hydrogen was used as fuel gas,

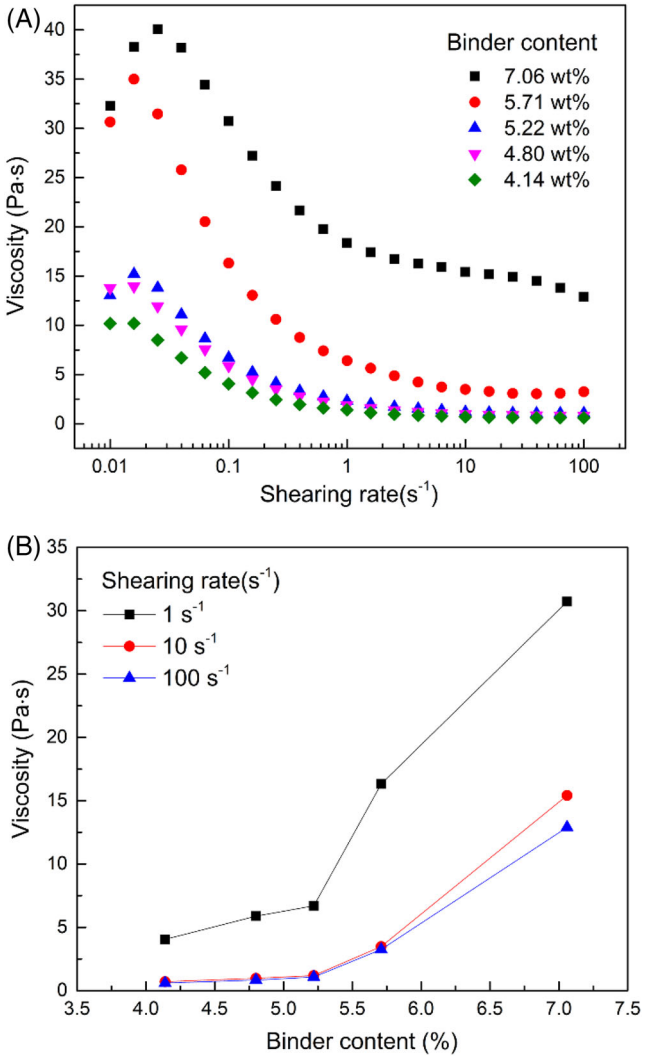


**FIGURE 2** Rheological properties of the suspensions derived from different binder amounts: (A) viscosity versus shearing rate and (B) viscosity versus binder amount

whereas ambient air was used as oxidant. Hydrogen flow rate was controlled at 50 mL $min^{-1}$ by a mass flow controller (APEX, Alicat Scientific, USA). The electrochemical performance of cells with LSCF cathode was tested using the same method as those with a Pt air electrode.

# 3 | RESULTS AND DISCUSSION

## 3.1 | Effect of binder amount on microstructure

The influence of binder amount in the slurry was investigated by changing the amount of PESf. During the preparation of the slurries, the solid loading was fixed at 70 wt.%. Figure 2 shows the relationship between the viscosity of the tape-casting slurry and the binder amount. At any

given PESf amount, the viscosity of the stainless steel slurry decreases with increasing the shear rate (Figure 2A). On the other hand, the viscosity of the slurry increases with increasing the binder concentration (Figure 2B). Note that for the slurry with low binder concentration, increase in the PESf amount leads to a slow increase in the slurry viscosity. However, when the binder amount reaches a critical value (5.22 wt.%), further increase in the binder amount will result in a sharp increase of the viscosity, demonstrating that the binder concentration has significant effects on the slurry viscosity. As the morphology of the metal support may be also related to the viscosity of tape slurry, a series of metallic supports with the binder amount of 4.14, 4.80, 5.22, 5.71 and 7.06 wt.% have been fabricated, denoted as M1, M2, M3, M4 and M5, respectively.

Figure 3 displays the microstructure of the metal supports fabricated with different binder amounts after sintered at 1250 °C for 3.5 h. It can be seen from Figure 3A–E that with the increase in the PESf concentration of the tape-casting slurry, the diameter of finger-like pores gradually decreases from 200 to 100 $\mu$m, whereas more finger-like pores are formed in the metal supports. In addition, the thickness of sponge-like layer decreases when adding more binder to the slurry. When the PESf amount is above 4.8 wt.%, the thickness of sponge-like layer is around 60 $\mu$m. The porosity of M1, M2, M3, M4 and M5 is 44.8%, 49%, 49.2%, 50.9% and 46.4%, respectively. These results are not similar to the previous report. Ren et al.[33] have indicated that the formation of finger-like pores is inhibited in the samples fabricated using high PESf concentration in the slurry. This may be due to the fact that the slurry was made from large particle size powders for phase-inversion tape casting in this study, and the sedimentation of solid powders in the slurry may influence the formation of the finger-like pores.

Figure 4 shows the gas permeability of the metal supports prepared with different binder amounts. The gas permeation performance of the metal support is improved by increasing the amount of PESf in the tape-casting slurry. However, further increasing the binder concentration (M4), the gas permeability has gradually reduced. The gas permeation result is directly related to the microstructure of the as-prepared metal supports. For support M1 derived from the slurry with 4.14 wt.% PESf, it has less finger-like pores and a thicker sponge-like layer, which may interfere with gas transport and consequently affect the total gas permeance. However, the orientation of the finger-like pores for the support M5 is not perpendicular to the support, which may interfere with gas transport and consequently affect the total gas permeance. Therefore, 430L metal support M3, which exhibits considerable porosity, highest gas permeability and desired microstructure, is suitable for MT-SOFCs application.

## 3.2 | Electrochemical performance of metal-supported SOFCs

Three plasma powers of 32, 36 and 40 kW were applied to fabricate ScSZ electrolytes, and the corresponding microstructures of the electrolyte coatings are shown in Figure 5. Figure 5A–C shows the cross-sectional microstructure of as-obtained half-cell after being polished. The NiO–ScSZ anode functional layer with a thickness of around 21 $\mu$m can be seen to adhere tightly to the metal support. With the increase in the plasma power, the thickness of the ScSZ electrolyte is increased from 35 to 55 $\mu$m. In addition, the amount of the apparent cracks and voids decreases with the increase in the plasma power. Higher plasma energy is expected to melt the ScSZ particles better, leading to a lower apparent coating porosity. The morphology of the fractured ScSZ coatings deposited at different plasma powers is shown in Figure 5a–c. Unbonded interfaces and cracks were present in the coatings at a plasma power of 32 and 36 kW. When the plasma power reaches 40 kW, the amount of unbonded interface decreases significantly. In addition, the continuous columnar structure was formed across the interlayer interface. Therefore, the plasma power has significant influence not only on the deposition efficiency, but also on the microstructure of the ScSZ electrolyte coating, and higher plasma power is more favorable to obtain desirable electrolyte coatings.

To study the gas tightness of the electrolyte, the open circuit voltage (OCV) of three types of half-cell assembly with a configuration of 430L/Ni-ScSZ/ScSZ was measured using 3 vol% $H_2O$-humidified hydrogen as fuel and ambient air as oxidant. The OCVs of the different half-cells as a function of test temperature and time are shown in Figure 6A and B, respectively. From Figure 6A, it can be seen that the OCVs of the half-cells improved with the increase in the plasma power at all cell operating temperatures. The OCV of the half-cells with the electrolyte deposited at 32 kW was 1.0 V at 700 °C, but it reached 1.05 V when the plasma power was increased to 40 kW. Apparently, this value is still lower than the theoretical OCV of 1.12 V,[34] indicating that the electrolyte is not completely dense. However, this is an acceptable value for SOFC operations and is significantly higher than that (~0.93 V) of cells with the ScSZ electrolyte obtained by APS reported in the literature,[35,36] in which the electrolyte was deposited at a longer spraying distance (100 mm), whereas the spraying distance for the electrolyte is usually about 70 mm in this study. To evaluate the stability of the half-cells, the OCV as a function of time was measured at 650 °C, as shown in Figure 6B. Rapid voltage drop was found for the half-cells with the ScSZ electrolyte obtained at the plasma power of 32 and 36 kW, which is likely due to the poor density of

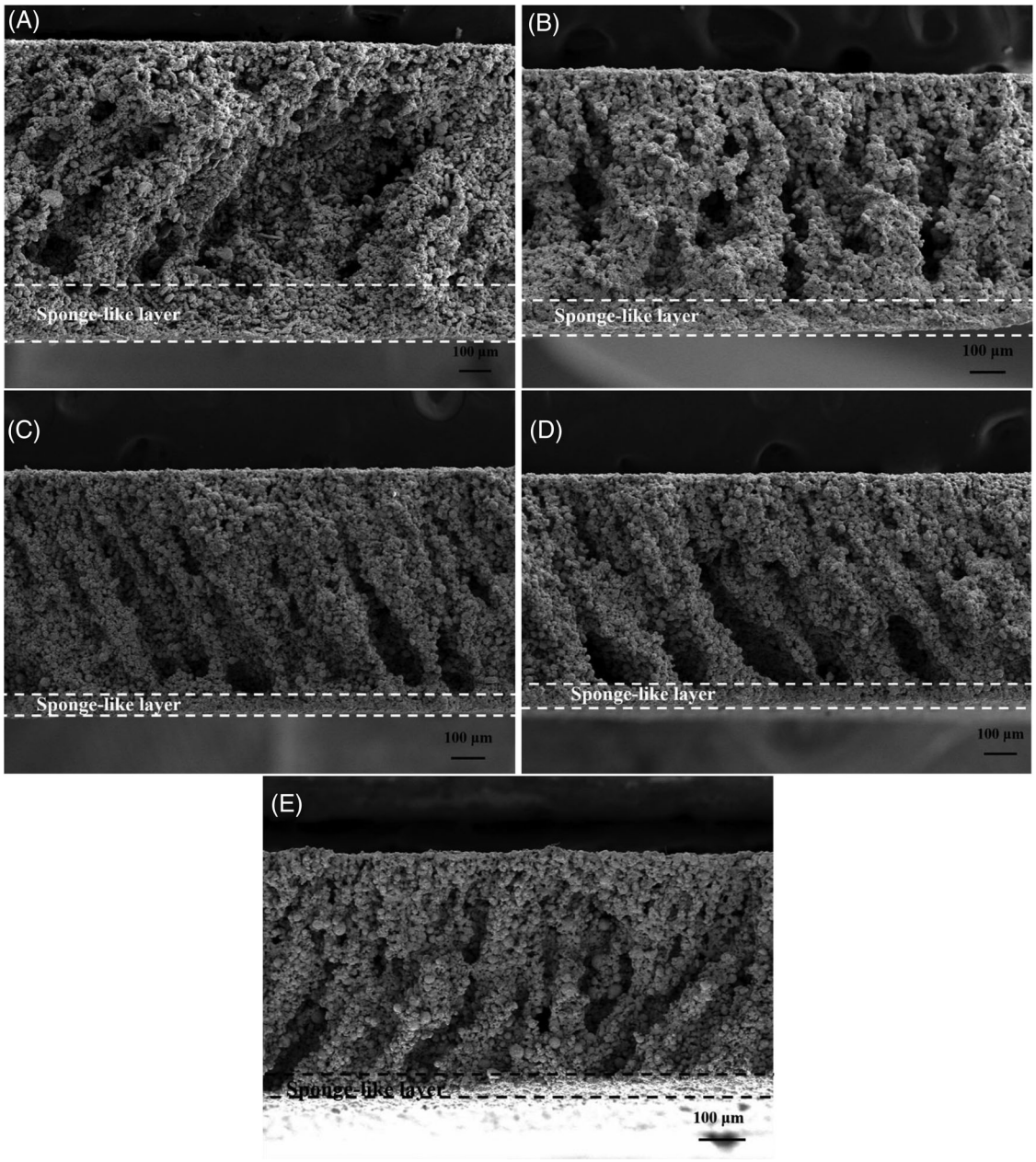


**FIGURE 3** Cross-sectional SEM images of the as-prepared 430L metal supports with different binder amounts: (A) 4.14 wt.%, (B) 4.80 wt.%, (C) 5.22 wt.%, (D) 5.71 wt.% and (E) 7.06 wt.%. SEM, scanning electron microscopy

the ScSZ electrolyte. By comparing the flow rates of the inlet and outlet of the gas stream, a significant leakage for these half-cells was observed. One potential reason may be due to the stress-relieving microcracks generated through the electrolytes at elevated temperatures.[19,37] There was no observable OCV degradation for the ScSZ electrolyte obtained at the plasma power of 40 kW, indicating that a relatively good gas-tight electrolyte layer is obtained by APS.

To investigate the correlation between the microstructure and the electrochemical performance of the MS-SOFCs, three types of MS-SOFCs with LSCF cathodes deposited at the plasma power of 6, 9 and 12 kW, and denoted as Cell 1, Cell 2 and Cell 3, respectively, were evaluated. SEM images of the cross sections of the polished LSCF cathode layer are shown in Figure 7, indicating that all the LSCF coatings were bonded well to the ScSZ electrolyte. As the plasma power was increased to deposit the LSCF cathode, the thickness of LSCF coatings was increased from 20 to 30 $\mu$m, whereas the amount of the pores in the LSCF cathode layer decreased significantly. Therefore, a lower plasma power (6 kW) was selected to produce the LSCF cathode coating, as the porosity is beneficial for facile mass transport of oxygen molecules to

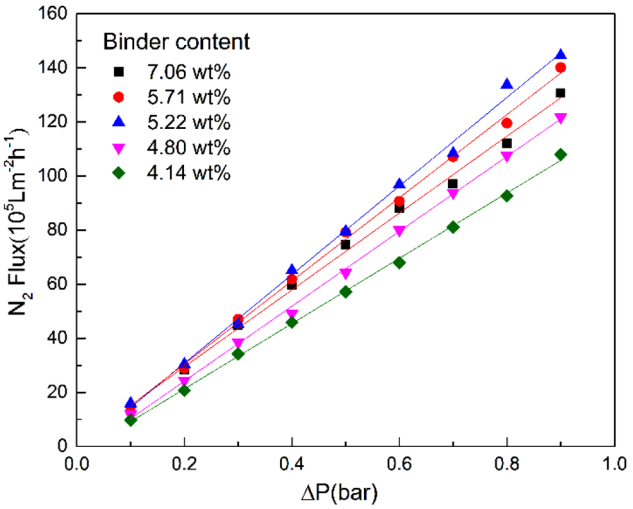


**FIGURE 4** Gas permeability of the metal supports from different binder amounts

the reaction sites in the mixed-conducting LSCF cathode to enlarge the reaction surface area.

Three types of MS-SOFCs, with the cell configuration of 430L/Ni-ScSZ/ScSZ/LSCF, were tested at 700 °C with humidified hydrogen (3 vol% $H_2O$) as fuel and ambient air as oxidant. Figure 8 shows the cell voltage and power density as a function of current density for the three types of MS-SOFCs. The OCVs of the three types of MS-SOFCs are all around 1.02 V, close to the corresponding half-cell value shown in Figure 6, indicating that the ScSZ electrolyte layers in all the three types of MS-SOFCs are dense enough to separate the fuel gas and air. The maximum power densities are 1079, 953 and 774 mW $cm^{-2}$ from Cell 1, Cell 2 and Cell 3, respectively. Although the metal support, the anode and the electrolyte of the three types of MS-SOFCs were prepared under identical conditions, it is reasonable to assume that the performance difference was due to the different microstructure features of the LSCF cathode

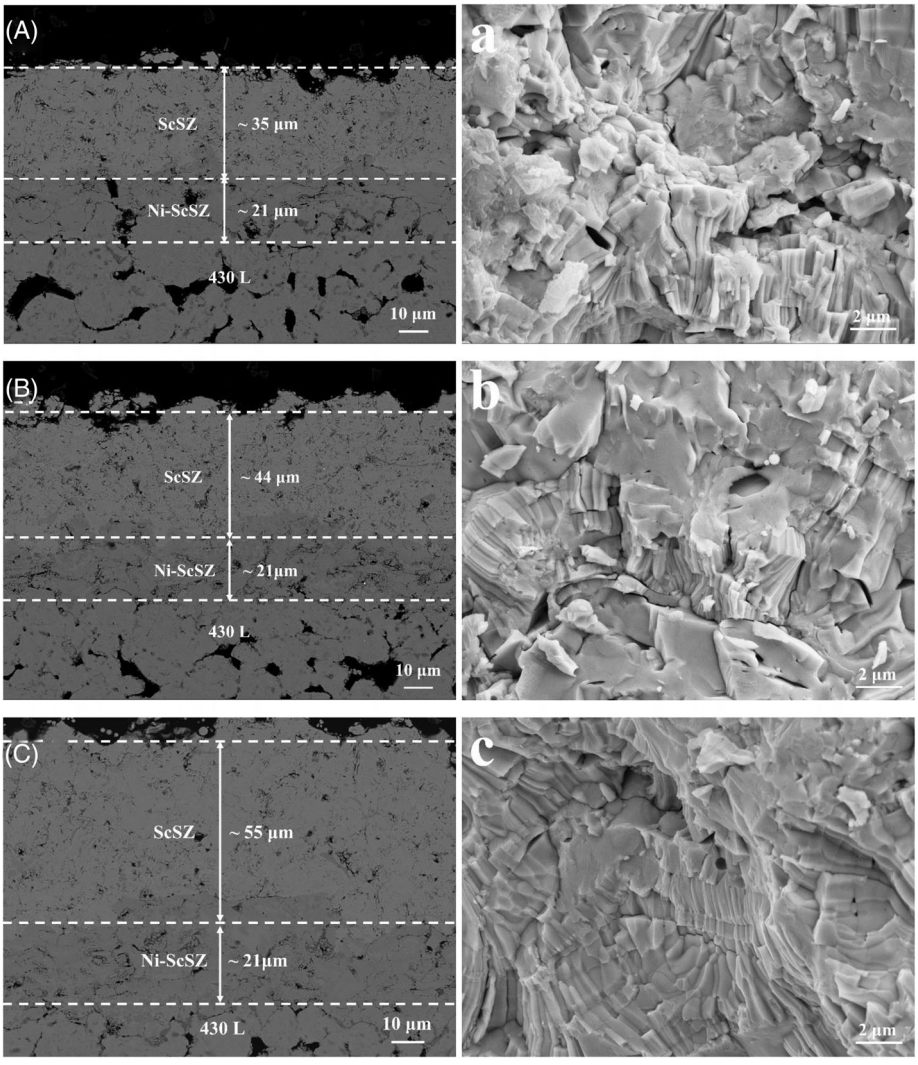


**FIGURE 5** SEM micrographs of a polished section (left) and a fractured surface (right) of ScSZ electrolyte layers deposited at different plasma powers: (A-a) 32 kW, (B-b) 36 kW and (C-c) 40 kW. ScSZ, scandia-stabilized zirconia; SEM, scanning electron microscopy

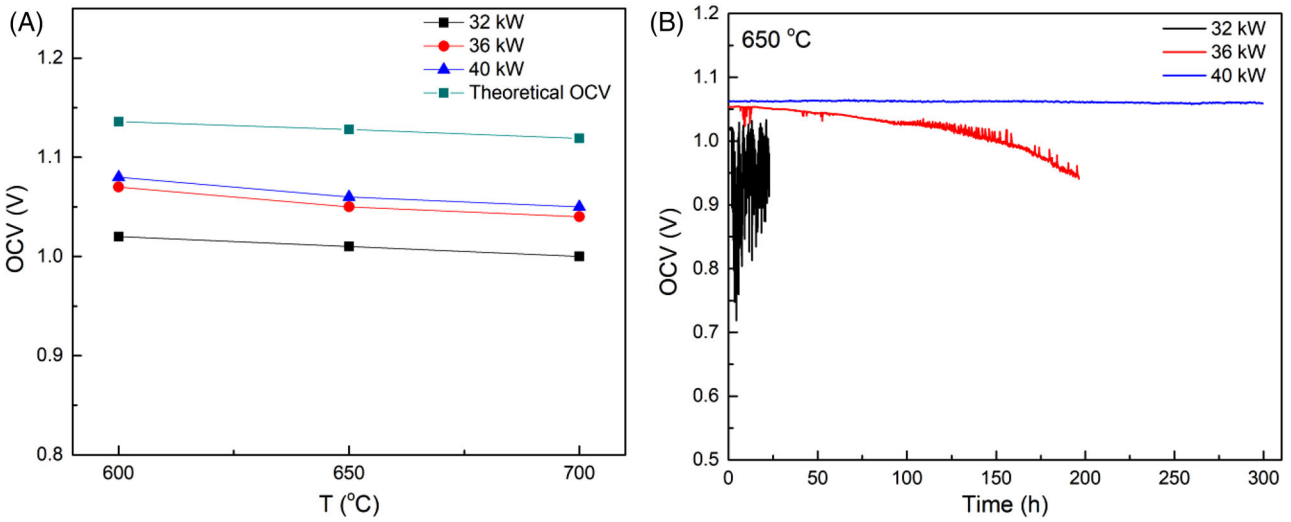


**FIGURE 6** (A) OCV of the half-cells with ScSZ fabricated at different plasma powers. (B) OCV of the half-cells versus time measured at 650 °C. ScSZ, scandia-stabilized zirconia; OCV, open circuit voltage

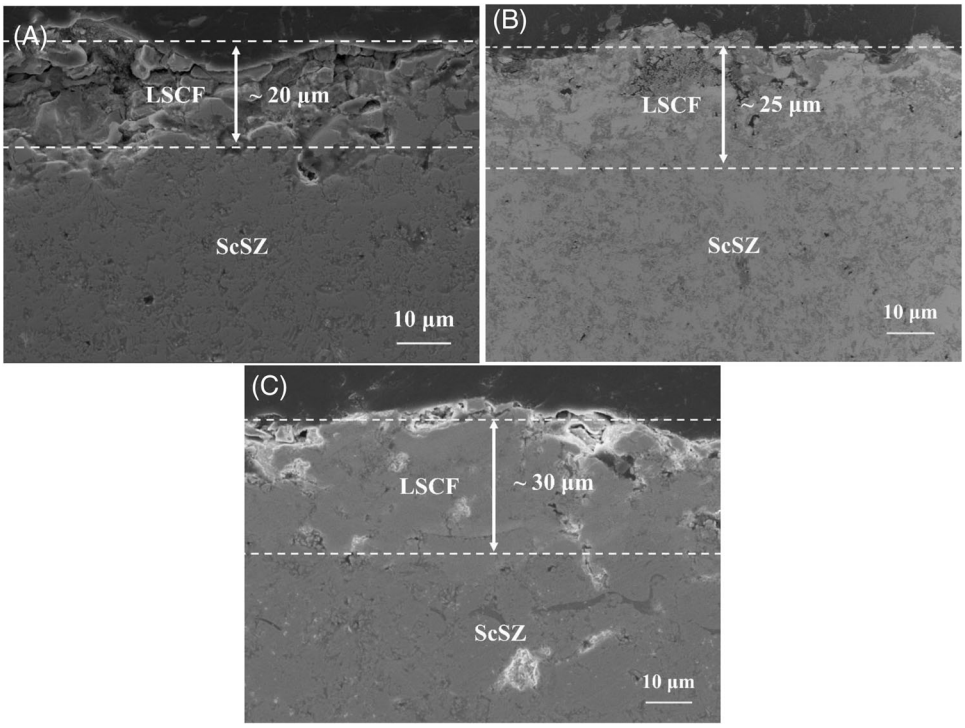


**FIGURE 7** SEM micrographs of the polished LSCF cathode layer deposited at different plasma power: (A) 6 kW, (B) 9 kW and (C) 12 kW. LSCF, $La_{0.6}Sr_{0.4}Co_{0.2}Fe_{0.8}O_{3-\delta}$; SEM, scanning electron microscopy

layer deposited by APS. The porous microstructure of the LSCF layer shown in Cell 1 is expected to improve the electrochemical reactions at the triple phase boundary. Furthermore, Cell 1 exhibits much higher cell performance compared to those of the MS-SOFCs with similar materials set but fabricated by APS on metal supports produced from the pore former method (Table 3). Such a difference in the cell performance could be attributed to the different microstructure features of the metal support. Metal support with open straight finger-like pores prepared by the phase-inversion tape-casting method is beneficial to mass transport, thus improving the cell performance and mitigating the concentration polarization.

Figure 9A shows the impedance spectra of three types of MS-SOFCs measured under OCV conditions at 700 °C. The high-frequency intercept corresponds to the ohmic

**TABLE 3** Comparison of electrochemical performance for MS-SOFCs by plasma spraying

| Cell configuration | Cell operating temperature (°C) | Maximum power density (mW cm$^{-2}$) | Ref. |
|---|---|---|---|
| Ni–YSZ/LSGM/LSCF | 700 | 170 | 38 |
| LDC–Ni/LDC/LSGM/LSGM-LSCF | 750 | 978 | 39 |
| Ni–YSZ/YSZ/BPCF | 750 | 610 | 40 |
| Ni–YSZ/YSZ/SDC-LSCF | 700 | 460 | 41 |
| NiO–YSZ/YSZ/SDC-LSCF | 750 | 500 | 42 |
| NiO–YSZ/LSGM/LSCF | 700 | 290 | 43 |
| NiO–ScSZ/ScSZ/LSCF | 700 | 754 | 44 |
| NiO–ScSZ/ScSZ/LSCF | 700 | 1079 | This study |

Abbreviation: MS-SOFC, metal-supported solid oxide fuel cell.

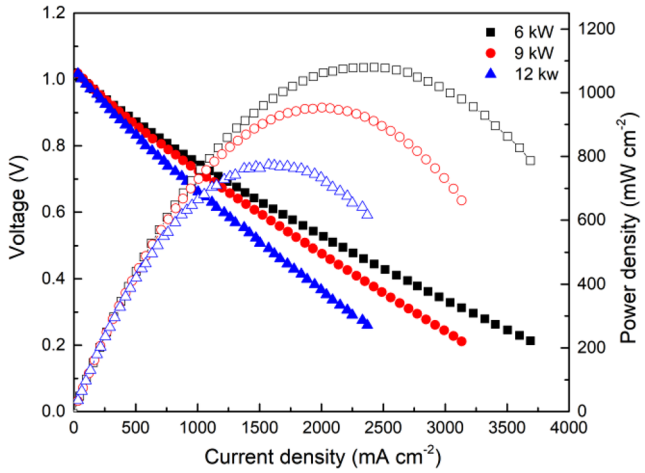


**FIGURE 8** Cell voltage and power density as function of current density for the MS-SOFCs tested at 700°C with humidified $H_2$ as fuel and ambient air as oxidant. MS-SOFC, metal-supported solid oxide fuel cell

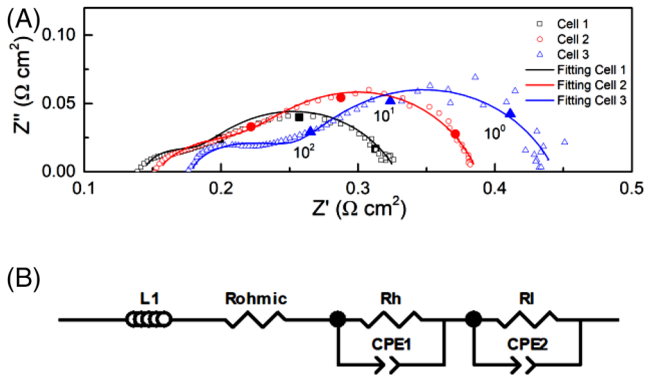


**FIGURE 9** (A) Impedance spectra for the cells measured under the OCV conditions at 700°C. The equivalent circuit for the electrode processes and the corresponding fitted curve were also included. (B) Equivalent circuit for the impedance fitting. OCV, open circuit voltage

**TABLE 4** The area-specific resistance values obtained by fitting the impedance spectra of the three types of MS-SOFCs

| Sample | Cell 1 | Cell 2 | Cell 3 |
|---|---|---|---|
| $R_H$ (Ω cm$^2$) | 0.04 | 0.08 | 0.09 |
| $R_L$ (Ω cm$^2$) | 0.14 | 0.15 | 0.18 |
| $R_p$ (Ω cm$^2$) | 0.18 | 0.23 | 0.27 |

Abbreviation: MS-SOFC, metal-supported solid oxide fuel cell.

resistance ($R_o$), whereas the low-frequency intercept represents the total resistance ($R_t$). The overall size of the impedance loop is attributed to the polarization resistance ($R_p$), including activation and concentration polarization resistances. From Figure 9A, the $R_o$ values for Cell 1, Cell 2 and Cell 3 were determined to be 0.14, 0.15 and 0.17 Ω cm$^{-2}$, respectively, and the corresponding $R_t$ values were 0.32, 0.39 and 0.44 Ω cm$^{-2}$, respectively. Apparently, the $R_p$ value increased from 0.18 to 0.27 Ω cm$^{-2}$ with the increase in the plasma power for depositing the LSCF cathode from 6 to 12 kW. Compared with the ohmic resistance, the polarization resistance varied more substantially with the plasma power used to deposit the LSCF cathode. Therefore, an equivalent circuit model was proposed to further analyze these impedance spectra. As shown in Figure 9B, the impedance spectra consist of two arcs: the high-frequency resistance ($R_H$) related to charge transfer process at the gas/electrode interface and the low-frequency resistance ($R_L$) that is normally ascribed to the surface adsorption/desorption and gas diffusion.[45] The fitting curves are shown in Figure 9A, and the values extracted from the curve fitting are summarized in Table 4. Both $R_H$ and $R_L$ increase with the plasma power for depositing the LSCF cathode. Although the metal support, the anode and the electrolyte are nominally identical, the difference in the polarization resistances for the various cells can be attributed to the microstructure difference in the cathode microstructure. The densification of

the LSCF cathode at higher plasma powers not only leads to less effective charge transfer due to the loss of active sites but also increases gas-diffusion resistance owing to insufficient porosity. In addition, it is apparent that $R_L$ dominates in the overall cell $R_p$, indicating that the adsorption/desorption and gas-diffusion process become the limiting step. Therefore, the electrochemical performance of the MS-SOFCs can be significantly improved by tailoring the microstructure of the cathode.

## 4 | CONCLUSION

In this study, planar MS-SOFCs with the cell configuration of 430L/Ni-ScSZ/ScSZ/LSCF have been successfully fabricated by the APS process on metal supports manufactured through the phase-inversion tape-casting method. The binder amount of the slurry can significantly influence the morphology of the metal support fabricated. The metal support with the desired microstructure could be tailored by adjusting the amount of the PESf binder in the slurry. Metal supports with large straight pores are beneficial to mass transport, thus mitigating the concentration polarization. The plasma power is a key factor in controlling the coating microstructures of the ScSZ electrolyte and the LSCF cathode by APS. Satisfactory gas-tight ScSZ electrolytes and porous LSCF cathodes were obtained by selecting a proper plasma power during the APS process. The optimized MS-SOFCs exhibited a maximum cell output power density of 1079 mW $cm^{-2}$ at 700 °C using humidified $H_2$ as fuel and ambient air as oxidant. The corresponding ohmic and total resistance of MS-SOFCs was 0.14 and 0.32 Ω $cm^2$, respectively, suggesting that APS is a promising approach for manufacturing high-performance MS-SOFCs.

### ACKNOWLEDGMENT

This work was supported by the US Department of Energy (DE-EE0009427 and DE-FE0031670).

### ORCID

*Peng Qiu* https://orcid.org/0000-0002-7397-2199
*Fanglin Chen* https://orcid.org/0000-0001-9942-8872

### REFERENCES

1. Tucker MC. Progress in metal-supported solid oxide fuel cells: a review. J Power Sources. 2010;195(15):4570–82.
2. Tucker MC. Durability of symmetric-structured metal-supported solid oxide fuel cells. J Power Sources. 2017;369:6–12.
3. Dewa M, Yu W, Dale N, Hussain AM, Norton MG, Ha S. Recent progress in integration of reforming catalyst on metal-supported SOFC for hydrocarbon and logistic fuels. Int J Hydrogen Energy. 2021;46(67):33523–40.
4. Sumi H, Yamaguchi T, Hamamoto K, Suzuki T, Fujishiro Y. Effects of anode microstructure on mechanical and electrochemical properties for anode-supported microtubular solid oxide fuel cells. J Am Ceram Soc. 2013;96(11):3584–8.
5. Connor PA, Yue X, Savaniu CD, Price R, Triantafyllou G, Cassidy M, et al. Tailoring SOFC electrode microstructures for improved performance. Adv Eng Mater. 2018;8(23):1800120.
6. Zhou Y, Meng X, Liu X, Pan X, Li J, Ye X, et al. Novel architectured metal-supported solid oxide fuel cells with Mo-doped $SrFeO_{3-\delta}$ electrocatalysts. J Power Sources. 2014;267:148–54.
7. Brandner M, Bram M, Froitzheim J, Buchkremer H, Stöver D. Electrically conductive diffusion barrier layers for metal-supported SOFC. Solid State Ionics. 2008;179(27–32):1501–4.
8. Kim KJ, Kim SJ, Choi GM. $Y_{0.08}Sr_{0.88}TiO_3$–$CeO_2$ composite as a diffusion barrier layer for stainless-steel supported solid oxide fuel cell. J Power Sources. 2016;307:385–90.
9. Ding D, Liu M, Liu Z, Li X, Blinn K, Zhu X, et al. Efficient electrocatalysts for enhancing surface activity and stability of SOFC cathodes. Adv Eng Mater. 2013;3(9):1149–54.
10. Fu YP, Subardi A, Hsieh MY, Chang WK. Electrochemical properties of $La_{0.5}Sr_{0.5}Co_{0.8}M_{0.2}O_{3-\delta}$ (M = Mn, Fe, Ni, Cu) perovskite cathodes for IT-SOFCs. J Am Ceram Soc. 2016;99(4):1345–52.
11. Meng Y, He W, Li X-x, Gao J, Zhan Z, Yi J, et al. Asymmetric $La_{0.6}Sr_{0.4}Co_{0.2}Fe_{0.8}O_{3-\delta}$ membrane with reduced concentration polarization prepared by phase-inversion tape casting and warm pressing. J Membr Sci. 2017;533:11–8.
12. Poulsen FW, van der Puil N. Phase relations and conductivity of Sr-and La-zirconates. Solid State Ionics. 1992;53:777–83.
13. Kim C, Kim S, Jang I, Yoon H, Song T, Paik U. Facile fabrication strategy of highly dense gadolinium-doped ceria/yttria-stabilized zirconia bilayer electrolyte via cold isostatic pressing for low temperature solid oxide fuel cells. J Power Sources. 2019;415:112–8.
14. Liu M, Uba F, Liu Y. A high-performance solid oxide fuel cell with a layered electrolyte for reduced temperatures. J Am Ceram Soc. 2020;103(9):5325–36.
15. Lenser C, Jeong H, Sohn YJ, Russner N, Guillon O, Menzler NH. Interaction of a ceria-based anode functional layer with a stabilized zirconia electrolyte: Considerations from a materials perspective. J Am Ceram Soc. 2018;101(2):739–48.
16. Wang L, Li C, Li C, Yang G. Performance of $La_{0.8}Sr_{0.2}Ga_{0.8}Mg_{0.2}O_3$-based SOFCs with atmospheric plasma sprayed La-doped $CeO_2$ buffer layer. Electrochim Acta. 2018;275:208–17.
17. Tsai C, Hwang C, Chang C, Wu S, Lin H, Shiu W, et al. Performances of plasma sprayed metal-supported solid oxide fuel cell and stack. Fuel Cells. 2018;18(6):800–8.
18. Vaßen R, Mack DE, Tandler M, Sohn YJ, Sebold D, Guillon O. Unique performance of thermal barrier coatings made of yttria-stabilized zirconia at extreme temperatures (>1500°C). J Am Ceram Soc. 2021;104(1):463–71.
19. Marr M, Kesler O. Permeability and microstructure of suspension plasma-sprayed YSZ electrolytes for SOFCs on various substrates. J Therm Spray Technol. 2012;21(6):1334–46.
20. Jiang P, Yang L, Sun Y, Li D, Wang T. Nondestructive measurements of residual stress in air plasma-sprayed thermal barrier coatings. J Am Ceram Soc. 2021;104(3):1455–64.
21. Liu G, Zhong X, Xing Y, Li T, Pan W. Surface resistivity and bonding strength of atmosphere plasma sprayed copper-coated alumina substrate. J Am Ceram Soc. 2021;104(3):1193–7.

22. Hermawan E, Lee GS, Kim GS, Ham HC, Han J, et al. Densification of an YSZ electrolyte layer prepared by chemical/electrochemical vapor deposition for metal-supported solid oxide fuel cells. Ceram Int. 2017;43(13):10450–9.
23. Hui SR, Yang D, Wang Z, Yick S, Decès-Petit C, Qu W, et al. Metal-supported solid oxide fuel cell operated at 400–600°C. J Power Sources. 2007;167(2):336–9.
24. Schiller G, Ansar A, Lang M, Patz O. High temperature water electrolysis using metal supported solid oxide electrolyser cells (SOEC). J Appl Electrochem. 2009;39(2):293–301.
25. Soysal D, Arnold J, Szabo P, Henne R, Ansar SA. Thermal plasma spraying applied on solid oxide fuel cells. J Therm Spray Technol. 2013;22(5):588–98.
26. Soysal D, Ansar A, Ilhan Z, Costa R. Nanostructured composite cathodes by suspension plasma spraying for SOFC applications. ECS Trans. 2011;35(1):2233.
27. Lin J, Chen L, Liu T, Xia C, Chen C, Zhan Z. The beneficial effects of straight open large pores in the support on steam electrolysis performance of electrode-supported solid oxide electrolysis cell. J Power Sources. 2018;374:175–80.
28. Dogdibegovic E, Wang R, Lau GY, Tucker MC. High performance metal-supported solid oxide fuel cells with infiltrated electrodes. J Power Sources. 2019;410–411:91–98.
29. Dong D, Shao X, Xie K, Hu X, Parkinson G, Li C-Z. Microchanneled anode supports of solid oxide fuel cells. Electrochem Commun. 2014;42:64–67.
30. Shi N, Su F, Huan D, Xie Y, Lin J, Tan W, et al. Performance and DRT analysis of P-SOFCs fabricated using new phase inversion combined tape casting technology. J Mater Chem A. 2017;5(37):19664–71.
31. Lin J, Miao G, Xia C, Chen C, Wang S, Zhan Z. Optimization of anode structure for intermediate temperature solid oxide fuel cell via phase-inversion cotape casting. J Am Ceram Soc. 2017;100(8):3794–800.
32. Liu T, Ren C, Zhang Y, Wang Y, Lei L, Chen F. Solvent effects on the morphology and performance of the anode substrates for solid oxide fuel cells. J Power Sources. 2017;363:304–10.
33. Ren C, Liu T, Mao Y, Maturavongsadit P, Luckanagul JA, Wang Q, et al. Effect of casting slurry composition on anode support microstructure and cell performance of MT-SOFCs by phase inversion method. Electrochim Acta. 2014;149:159–66.
34. Shi H, Ding Z, Ma G. Electrochemical performance of cobalt-free $Nd_{0.5}Ba_{0.5}Fe_{1-x}Ni_xO_{3-\delta}$ cathode materials for intermediate temperature solid oxide fuel cells. Fuel Cells. 2016;16(2):258–62.
35. Zhang S-L, Yu H-X, Li C-X, Lai SY, Li C-J, Yang G-J, et al. Thermally sprayed high-performance porous metal-supported solid oxide fuel cells with nanostructured $La_{0.6}Sr_{0.4}Co_{0.2}Fe_{0.8}O_{3-\delta}$ cathodes. J Mater Chem A. 2016;4(19):7461–8.
36. Yuan K, Song C, Chen G, Xu Z, Peng H, Lu X, et al. Preparation of dense ScSZ thin films by plasma spraying with densified ScSZ powders. Int J Hydrogen Energy. 2021;46(15):9749–57.
37. Bengtsson P, Johannesson T. Characterization of microstructural defects in plasma-sprayed thermal barrier coatings. J Therm Spray Technol. 1995;4(3):245–51.
38. Hwang C, Tsai C-H, Lo C-H, Sun C-H. Plasma sprayed metal supported YSZ/Ni–LSGM–LSCF ITSOFC with nanostructured anode. J Power Sources. 2008;180(1):132–42.
39. Hwang C-s, Tsai C-H, Yu J-F, Chang C-L, Lin J-M, Shiu Y-H, et al. High performance metal-supported intermediate temperature solid oxide fuel cells fabricated by atmospheric plasma spraying. J Power Sources. 2011;196(4):1932–9.
40. Wang Y, Legoux JG, Neagu R, Hui S, Marple BR. Suspension plasma spray and performance characterization of half cells with NiO/YSZ anode and YSZ electrolyte. J Therm Spray Technol. 2011;21(1):7–15.
41. Metcalfe C, Kuhn J, Kesler O. Characterization of Ni–YSZ anodes for solid oxide fuel cells fabricated by suspension plasma spraying with axial feedstock injection. J Power Sources. 2013;243:172–80.
42. Harris J, Kuhn J, Kesler O. Atmospheric plasma-sprayed metal-supported solid oxide fuel cells with varying cathode microstructures. ECS Trans. 2015;68(1):1779.
43. Zhang S-L, Liu T, Li C-J, Yao S-W, Li C-X, Yang G-J, et al. Atmospheric plasma-sprayed $La_{0.8}Sr_{0.2}Ga_{0.8}Mg_{0.2}O_3$ electrolyte membranes for intermediate-temperature solid oxide fuel cells. J Mater Chem A. 2015;3(14):7535–53.
44. Wang Y, Gao J, Chen W, Li C, Zhang S, Yang G, et al. Development of ScSZ electrolyte by very low pressure plasma spraying for high-performance metal-supported SOFCs. J Therm Spray Technol. 2020;29(1):223–31.
45. Wang C, Lü Z, Su C, Li J, Cao Z, Zhu X, et al. Effects of discharge mode and fuel treating temperature on the fuel utilization of direct carbon solid oxide fuel cell. Int J Hydrogen Energy. 2019;44(2):1174–81.


**How to cite this article:** Lin J, Li H, Wang W, Qiu P, Tao G, Huang K, et al. Atmospheric plasma spraying to fabricate metal-supported solid oxide fuel cells with open-channel porous metal support. J Am Ceram Soc. 2023;106:68–78. https://doi.org/10.1111/jace.18450